Resolving the Stellar-Collapse and Hierarchical-Merger Origins of the Coalescing Black Holes

Yin-Jie Li,[1,*] Yuan-Zhu Wang,[2,1,*] Shao-Peng Tang,[1] and Yi-Zhong Fan[1,3,†]
[1]Key Laboratory of Dark Matter and Space Astronomy, Purple Mountain Observatory, Chinese Academy of Sciences, Nanjing 210023, People's Republic of China
[2]Institute for Theoretical Physics and Cosmology, Zhejiang University of Technology, Hangzhou, 310032, People's Republic of China
[3]School of Astronomy and Space Science, University of Science and Technology of China, Hefei, Anhui 230026, People's Republic of China

(Received 12 April 2024; revised 27 May 2024; accepted 28 June 2024; published 1 August 2024)

Spin and mass properties provide essential clues in distinguishing the origins of coalescing black holes (BHs). With a dedicated semiparametric population model for the coalescing binary black holes (BBHs), we identify two distinct categories of BHs among the GWTC-3 events, which is favored over the one population scenario by a logarithmic Bayes factor ($\ln \mathcal{B}$) of 7.5. One category, with a mass ranging from $\sim 25 M_\odot$ to $\sim 80 M_\odot$, is distinguished by the high spin magnitudes (~ 0.75) and consistent with the hierarchical merger origin. The other category, characterized by low spins, has a sharp mass cutoff at $\sim 40 M_\odot$, which is natural for the stellar-collapse origin and in particular the pair-instability explosion of massive stars. We infer the local hierarchical merger rate density as $0.46^{+0.61}_{-0.24}$ Gpc^{-3} yr^{-1}. Additionally, we find that a fraction of the BBHs has a cosine-spin-tilt-angle distribution concentrated preferentially around 1, and the fully isotropic distribution for spin orientation is disfavored by a $\ln \mathcal{B}$ of -6.3, suggesting that the isolated field evolution channels are contributing to the total population.

DOI: 10.1103/PhysRevLett.133.051401

Introduction—Thanks to the excellent performance of the LIGO/Virgo network, about 90 gravitational wave (GW) events have been officially reported so far, and most of them are coalescing binary black holes (BBHs) [1–4]. The origins and evolution paths of these binaries, however, are still under debate [5–7].

As a result of the (pulsational) pair-instability supernova [(P)PISN] explosions [8,9], the BHs formed by stellar evolutions are expected to be absent in the so-called upper-mass gap (UMG), which is widely anticipated to start at ~ 40–$55 M_\odot$, though the threshold may be shifted under some special circumstances [9–15]. However, the hierarchical mergers in dynamical environments [5,6,16,17], the stellar mergers [18,19] and primordial BHs [20,21] may populate the UMG, and make it invisible. In general, the hierarchical merger-formed BHs are distinguishable from those born in stellar explosions for their high spin magnitudes (with a typical value of ~ 0.7) [16,22,23]. Therefore, it is possible to distinguish the category of higher-generation (HG) BHs via analyzing the mass versus spin-magnitude distribution for BHs from GW observations, and simultaneously constrain the lower-edge of the UMG (if it was not contaminated significantly by other exotic BHs). A UMG-like high-mass cutoff at $\sim 45 M_\odot$ favored by the GWTC-1 data [10,24] had been challenged by further observations and, in particular, GW190521 [25], which suggested the absence of mass cutoff till $\gtrsim 80 M_\odot$ [26–28]. Some parametric investigations anyhow found that the UMG may still exist [29–33] and there may be hierarchical mergers [34–36], under some special astrophysical assumptions (e.g., single channel for all the BBHs). Such conclusions are however not confirmed by the non- or semiparametric approaches (with minimal assumptions) [7,37–40]. To reliably clarify the situation, *for the first time,* we propose a mixture flexible population model incorporating the correlation in the component-mass versus spin-magnitude distribution, to explore the subpopulations or groups of the coalescing BHs, and hence determine the origins and evolution channels of the BBHs.

Population model—Since coalescing BHs with diverse origins may have different component-mass (m) and spin-magnitude (χ) distributions, we use a mixture model for m-χ distribution, which reads

$$\pi(m,\chi|\mathbf{\Lambda}) = \sum_{i=1}^{N} \pi_i(m,\chi|\mathbf{\Lambda}_i) \times r_i, \tag{1}$$

where r_i is the mixing fraction of the i-th component. Different from previous approaches modeling on the chirp-mass, mass-ratio, and aligned-spin distributions [38,41,42],

*These authors contributed equally to this letter.
†Contact author: yzfan@pmo.ac.cn

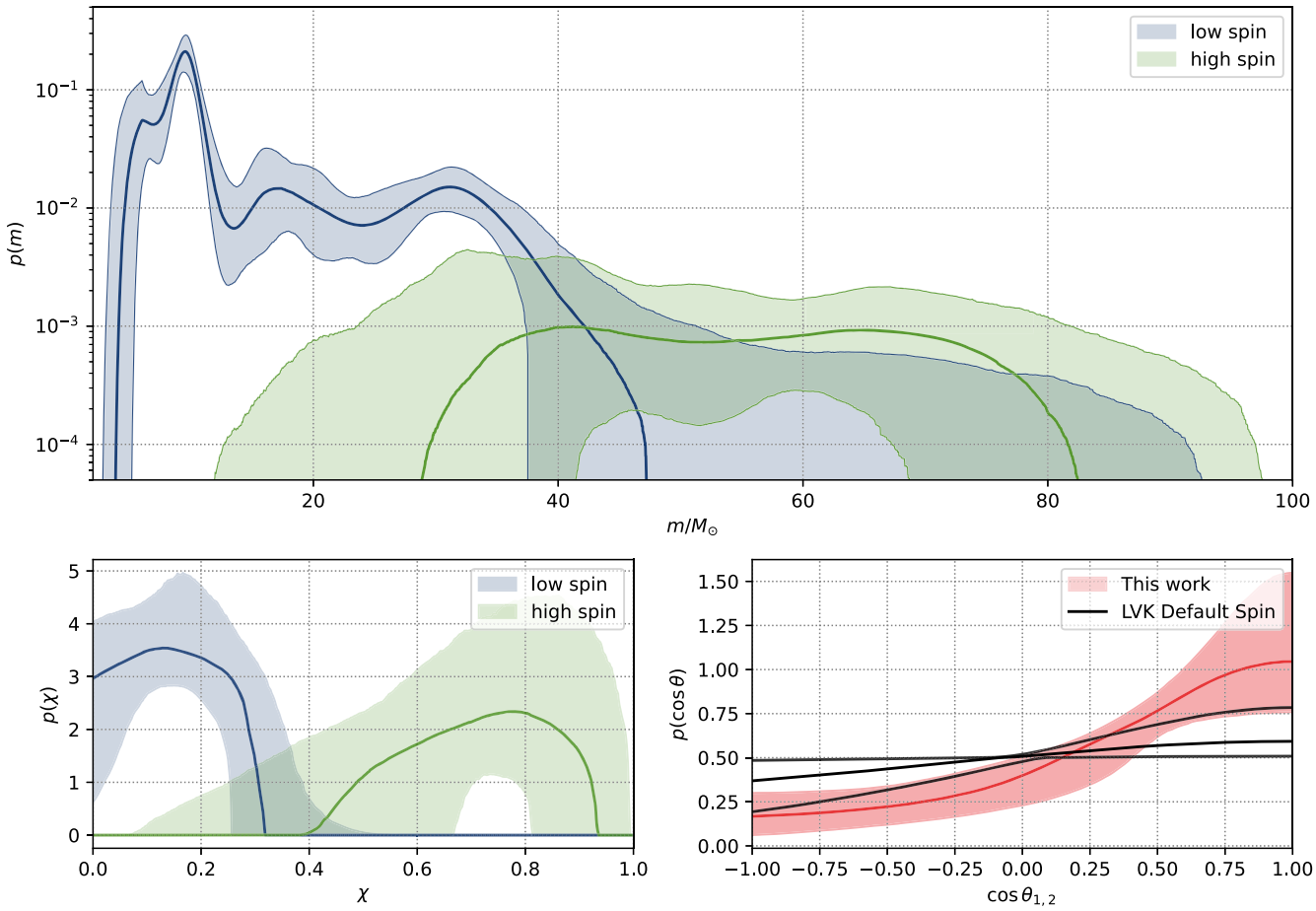

FIG. 1. Reconstructed mass (top) and spin (bottom) distribution of BHs; the solid curves are the medians and the colored bands are the 90% credible intervals; note the spin-magnitude distribution of each subpopulation is normalized.

our model is more appropriate to investigate the subpopulations of *individual* BHs (in coalescing systems), and hence to identify the subpopulations in the BBHs. The m-χ distribution of the ith component is

$$\pi_i(m,\chi|\mathbf{\Lambda}_i) = \mathcal{PS}[m|\alpha_i, m_{\min,i}, m_{\max,i}, \delta_i, f_i(m;\{f_i^j\}_{j=0}^{N_{\rm knot}})] \times \mathcal{G}(\chi|\chi_{\min,i},\chi_{\max,i},\mu_{\chi,i},\sigma_{\chi,i}), \quad (2)$$

where $\mathcal{PS}$ is a one-dimensional PowerLawSpline model [27], which provides a flexible and continuous function, thus is appropriate to determine the underlying mass distributions of the BHs in different categories if distinguishable; $f_i(m)$ is the cubic-spline perturbation function interpolated between $N_{\rm knot}$ knots placed in the mass range. We use 12 knots (The number of the knots does not affect our conclusions, see Fig. S27 of Supplemental Material [43].) to interpolate the perturbation function f_i, located linearly in the logarithm space within [6,59] $M_\odot$, and restrict the perturbation to zero at the minimum and maximum knots. $\mathcal{G}$ is a truncated Gaussian within the range of $[\chi_{\min,i},\chi_{\max,i}]$ with a central value ($\mu_{\chi,i}$) and a standard deviation ($\sigma_{\chi,i}$).

As found previously, the two objects in a BBH are not randomly paired [60,61]. The pairing functions for different channels (e.g., the dynamical and field channels) may not be the same [36,41]. However, currently we cannot robustly differentiate the formation channel of most BBHs. Therefore, we take a simple pairing function of $(m_2/m_1)^\beta$. Anyhow, even for the unpaired (or randomly paired, i.e., $\beta = 0$) scenario, our results are unchanged, implying that our findings are insensitive to the pairing function (see Sec. VII in the Supplemental Material [43]).

The cosine-tilt-angle distribution reads [7]

$$\begin{aligned}&\mathcal{GU}(\cos\theta_1,\cos\theta_2|\zeta,\sigma_t)\\ &= \mathcal{G}(\cos\theta_1|-1,1,1,\sigma_t)\times\mathcal{G}(\cos\theta_2|-1,1,1,\sigma_t)\times\zeta\\ &\quad + (1-\zeta)\times\mathcal{U}(\cos\theta_1|-1,1)\times\mathcal{U}(\cos\theta_2|-1,1),\end{aligned} \quad (3)$$

where $\mathcal{U}$ is the uniform distribution between -1 and 1, and $\mathcal{G}$ is the (normalized) Gaussian distribution truncated between -1 and 1. Following Abbott *et al.* [7], the merger rate density evolution function is taken as $\mathcal{R} \propto (1+z)^{2.7}$. The final population model takes the form of

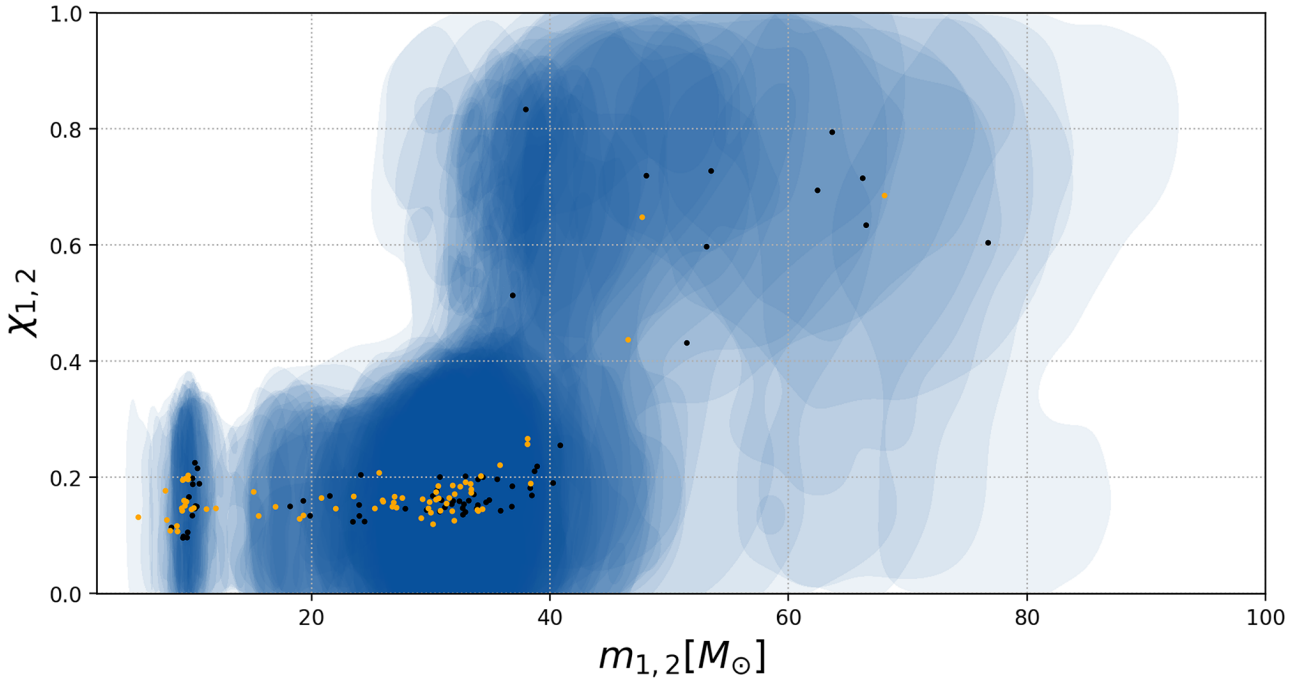

FIG. 2. Posteriors of individual component masses and spin magnitudes of BBHs in GWTC-3 reweighted to a population-informed prior inferred by the fiducial model. The shaded areas mark the 90% credible regions and the black (orange) points stand for the mean values for the primary (secondary) BHs. The difference between the two groups is evident: the first group is lighter than $\sim 50 M_\odot$ with spin magnitudes $\lesssim 0.3$, while the second group extends to the higher mass range and has a typical spin magnitude ~ 0.7.

$$\begin{aligned}&\pi(\lambda|\mathbf{\Lambda};\zeta,\sigma_t,\beta)\\&= C(\mathbf{\Lambda};\beta)\times\pi(m_1,\chi_1|\mathbf{\Lambda})\times\pi(m_2,\chi_2|\mathbf{\Lambda})\times(m_2/m_1)^\beta\\&\quad\times\Theta(m_1-m_2)\times\mathcal{GU}(\cos\theta_1,\cos\theta_2|\zeta,\sigma_t)\times p(z|\gamma=2.7),\end{aligned}\tag{4}$$

where $C(\mathbf{\Lambda};\beta)$ is the normalized function, and $\Theta(m_1-m_2)$ is Heaviside function. All hyperparameters are described in Table I in the Supplemental Material [43].

Results—We have performed hierarchical inferences and Bayesian model comparisons (see Secs. I, II, III, and IV of the Supplemental Material [43]). It reveals two groups of BHs with significantly different spin-magnitude distributions and mass distributions (see Fig. 1), which are evidently illustrated by the posterior distributions of the observed events weighted by the population-informed priors obtained by our two-component model (see Fig. 2). The two categories or groups of BHs are clear and identifiable. For the spin-magnitude distributions, the first group (hereafter the low-spin group; LSG) peaks at $0.14^{+0.13}_{-0.12}$ and terminates at $0.32^{+0.43}_{-0.06}$ (hereafter the values are for the median value and the 90% symmetric interval, unless otherwise noted), while in the second group (hereafter the high-spin group; HSG), the spin-magnitude distribution starts at $0.36^{+0.30}_{-0.31}$, peaks at $0.75^{+0.17}_{-0.27}$ and ends at $0.93^{+0.06}_{-0.12}$. The significantly different spin-magnitude distributions between the two groups indicates the different physical origins [16]. For the mass distributions, the LSG (HSG) starts at $3.26^{+1.53}_{-0.108} M_\odot$ ($27.16^{+12.98}_{-19.49} M_\odot$) and terminates at $47.26^{+45.90}_{-9.81} M_\odot$ ($82.74^{+14.86}_{-14.29} M_\odot$) with an overall power-law index of $2.10^{+1.05}_{-1.17}$ ($0.82^{+4.22}_{-3.40}$). The posterior of other parameters for the mass and spin distributions is displayed in the Figs. S20 and S21 in the Supplemental Material [43].

(i)—Evidence for hierarchical mergers—As shown in the Fig. 1, the spin-magnitude distribution of HSG (blue dashed region) is peaked at $\sim$0.6–0.8, which could be naturally associated with the spin distribution of the remnants of BBH mergers [22,23]. With the identification of the HSG as the HG category, we estimate that hierarchical mergers (containing at least one HG BH) take a fraction of $2.6^{+3.7}_{-1.5}\%$, and $0.39^{+0.74}_{-0.27}\%$ of the sources have two HG BHs (see Fig. S26 in Supplemental Material [43]). Such fractions may be too high to be realistic for the globular clusters alone [62], thus the contributions from the nuclear star clusters [63] and/or the accretion disks of active galactic nuclei (AGN) [17,64,65] may be needed. Assuming the merger rate of BBHs evolves with the redshift as $\propto (z+1)^{2.7}$, as obtained by Abbott *et al.* [7], we infer the local hierarchical merger rate density as $0.46^{+0.61}_{-0.24}\ \mathrm{Gpc^{-3}\,yr^{-1}}$. Additionally, we have identified events with probabilities $> 50\%$ to be hierarchical mergers (summarized in Table IV of the Supplemental Material [43]). In particular, GW190521 and GW191109_010717 have probabilities $> 50\%$ to host double HG BHs.

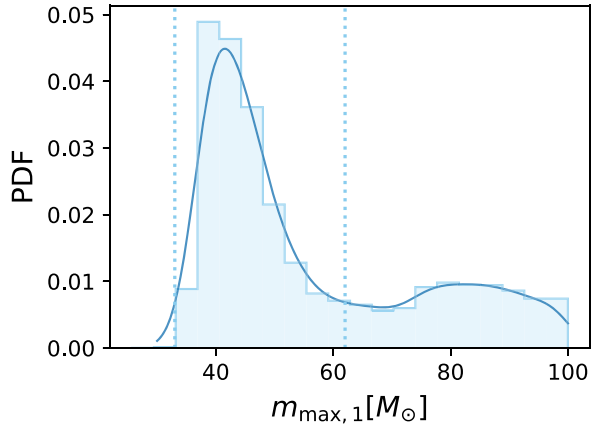

FIG. 3. Posterior of the maximum-mass cutoff of the LSG, the 68.3% (1σ) minimal credible intervals are indicated by dashed line; $m_{\mathrm{max},1}$ has a tail extending to the higher mass range, which may be caused by the flexibility of the PowerLawSpline mass model, see detailed discussion in Sec. VIII B. of the Supplemental Material [43].

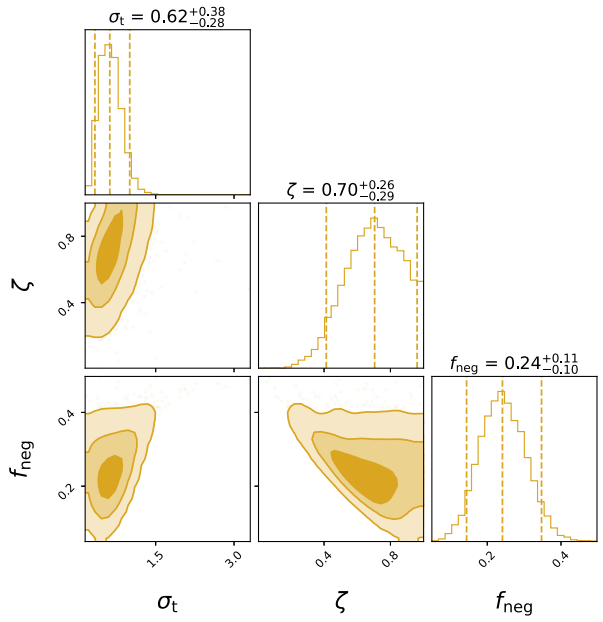

FIG. 4. Posterior distribution of σ_t, ζ, and the antialigned fraction f_{neg}; the dashed and solid contours mark the central 50% and 90% posterior credible regions, respectively.

(ii)—Evidence for pair-instability supernovae explosions—Apart from the HG category, the remaining BHs (i.e., the LSG) belongs to the stellar-collapse category. There is a rapid decline after $\sim 40M_\odot$ in the mass function of the LSG, as shown in Fig. 1, which supports the existence of the UMG caused by the (P)PISN [8,9]. Indeed, we have $m_{\mathrm{max},1} = 41.56^{+20.46}_{-8.55} M_\odot$ (the 1σ minimal credible interval, as shown in Fig. 3), which is in good agreement with the maximum mass of the stellar-formed BHs predicted by stellar evolution theories [10–12], as well as the results inferred with astrophysical-motivated parametric model and the deep-learning model [36,66]. The mass of the 99% (99.5%) percentile for the first-generation is $37.42^{+4.29}_{-2.96} M_\odot$ ($39.61^{+8.70}_{-3.79} M_\odot$), see Fig. S24 in Supplemental Material [43]. The $m_{\mathrm{max},1}$ has a tail caused by the flexibility of the PowerLawSpline model, as illustrated by the Fig. S23 in Supplemental Material [43]. Abbott *et al.* [7] suggest that either the UMG presents above $75M_\odot$ or there is a non-negligible fraction of the high-mass binaries formed in a way that avoids pair instability. The latter is in agreement with our interpretation.

(iii)—The spin-orientation distribution of BBHs—We find a fraction ($\zeta = 0.70^{+0.26}_{-0.29}$) of the BBHs has a cosine-spin-tilt-angle distribution peaking at 1 with width of $\sigma_t = 0.62^{+0.38}_{-0.28}$ (see Fig. 4), consistent with the isolated field BBHs [67]. We estimate that $24^{+11}_{-10}\%$ of BHs have spin-tilt angles $> 90°$. Flatter distributions of $\cos\theta$ have been reported in [7], whereas we find the fully isotropic spin-orientation distribution is disfavored by $\ln \mathcal{B} = -6.3$. The difference between our results and the previous [7,68] is mainly attributed to the different configurations for the Monte Carlo integral in likelihood estimation and the different modeling of spin-magnitude versus mass distribution (see Sec. VI of Supplemental Material [43] for more details). Vitale *et al.* [68] found that the $\cos\theta$ distribution may not peak at ~ 1. For comparison, we perform an inference with a variable μ_t for the Two-component model, and obtain $0.79^{+0.19}_{-0.29}$ (see Fig. S14 in Supplemental Material [43]). It is worth noticing that the modeling of the tilt-angle distribution does not affect the identification of the two subpopulations of BHs in this work (see Sec. VII of Supplemental Material [43]).

We have further investigated the $\cos\theta$ distributions in the two subpopulations, and it shows that, beside the first-generation subpopulation, the HG subpopulation may also have a fraction of nearly aligned assembly. Nevertheless, the fully isotropic distribution for the HG subpopulation cannot be ruled out yet (see Sec. IX of Supplemental Material [43] for details).

Conclusion and discussion—We investigate the population properties of BBHs in the GWTC-3, with a flexible semi-parametric population model. For the first time, we identify two subpopulations of coalescing BHs (with a $\ln \mathcal{B} = 7.5$ comparing to the one-component model), which are nicely consistent with the widely discussed hierarchical mergers [16] and the pair-instability mass gap (PIMG) [69,70]. These two issues are currently of great concern in gravitational-wave astronomy [5,7,9,16].

It was found that the unequal-mass BBHs have larger effective spins [7,71]. The hierarchical mergers identified in this work may explain such an anticorrelation between q-χ_{eff} (see Fig. S30 of the Supplemental Material [43]). Fishbach and Kalogera [72] found that the observed spins in x-ray binaries (XRBs) [73] are in tension with the BBH

spin distribution at the $> 99.9\%$ level. When we only account for the first-generation BBHs (i.e., the LSG), such tension would be more significant, indicating the lack of shared evolutionary paths between the two types of systems [74]. The spin-magnitude distribution of HSG can partially overlap with that of the XRB BHs, however, there is significant tension between their mass distributions [75].

Kimball *et al.* [35] reported evidence for hierarchical mergers in GWTC-2. However, their population model consists of a specific mass function and a fixed spin-magnitude distribution for higher-generation BHs, assuming that all BBHs were formed dynamically in gravitationally bound clusters, which seems unnatural [41]. Many other flexible semi- or nonparametric population models [7,38–40,76] have been used to fit the GWTC-3 data, but none of these approaches has taken into account the correlation in the component-mass versus spin-magnitude distribution and hence drawn different conclusions from us.

After posting our initial version online, other semi or nonparametric population models have also been developed to explore the subpopulations within the GWTC-3, see Godfrey *et al.* [77] and Ray *et al.* [78]. Although some findings of these two studies align with ours, neither provides evidence for a subpopulation with $\chi \sim 0.7$ or a mass cutoff at $\sim 40 M_{\odot}$. Different from us, Godfrey *et al.* [77] assumes that both spin magnitudes of a BBH follow the same distribution. While discrepancies between our findings and those of Ray *et al.* [78] likely arise from different approaches in modeling population parameters: we focus on spin magnitudes and orientations, while they concentrate on effective spins.

Gerosa and Fishbach [16] proposed that investigating the occurrence of hierarchical mergers constitutes an orthogonal and complementary direction to the usual "field versus dynamics" formation-channel debate. The route to the former issue usually depends on the spin-magnitude distributions [22,23], while the latter mainly relies on the spin-orientation distributions [67,79]. Our subsequent research [80], building on the identification of hierarchical mergers in this study, shows that BBH components in the $10 M_{\odot}$ and $35 M_{\odot}$ peaks of the primary-mass distribution exhibit nearly aligned and isotropic spin orientations, respectively. These orientations correspond to field and dynamic formation channels, aligning with the properties reported in Godfrey *et al.* [77], Ray *et al.* [78] for the respective peaks.

Encouragingly, hundreds of observations are promising after the next observing run [59], so that the origins and formation channels may be clearly identified. Additionally, the location of the PIMG will be measured more precisely, which can help constrain the $^{12}\mathrm{C}(\alpha,\gamma)^{16}\mathrm{O}$ in the stellar evolution theories [11]. Subsequently, one can even measure the lower edge of the PIMG evolving with the red shift, and hence the metallicity evolving with the age of the Universe [14]. Moreover, the lower edge of PIMG provides essential ingredients for measuring the expansion rate $[H(z)]$ of the Universe, via so-called "spectral sirens" [81–84]. With the significantly enriched GW data, more subpopulations of BHs/BBHs and features in each subpopulation may be revealed, which are not identified with current data using more complex population models as introduced in Sec. II of the Supplemental Material [43].

Acknowledgments—This work was supported in part by the NSFC under Grants of No. 12233011, No. 11921003 and No. 12203101, the Strategic Priority Research Program of the Chinese Academy of Sciences (No. XDB0550400), and the General Fund (No. 2023M733736) and the Postdoctoral Fellowship Program (GZB20230839) of the China Postdoctoral Science Foundation. We thank Yong-Jia Huang for discussion. This research has made use of data and software obtained from the Gravitational Wave Open Science Center [86], a service of LIGO Laboratory, the LIGO Scientific Collaboration and the Virgo Collaboration. LIGO is funded by the U.S. National Science Foundation. Virgo is funded by the French Centre National de Recherche Scientifique (CNRS), the Italian Istituto Nazionale della Fisica Nucleare (INFN) and the Dutch Nikhef, with contributions by Polish and Hungarian institutes. The publicly available code GWPopulation [87] is referenced in calculating the variance of log-likelihood in the Monte Carlo integrals.

Data availability—The codes used for this work are publicly available in GitHub [85].

[1] B. P. Abbott, R. Abbott, and T. D. Abbott, Phys. Rev. X **9**, 031040 (2019).
[2] R. Abbott, T. D. Abbott, and S. Abraham, Phys. Rev. X **11**, 021053 (2021).
[3] R. Abbott, T. D. Abbott, and F. Acernese, Phys. Rev. D **109**, 022001 (2024).
[4] R. Abbott, T. D. Abbott, and F. Acernese, Phys. Rev. X **13**, 041039 (2023).
[5] I. Mandel and A. Farmer, Phys. Rep. **955**, 1 (2022).
[6] I. Mandel and F. S. Broekgaarden, Living Rev. Relativity **25**, 1 (2022).
[7] R. Abbott, T. D. Abbott, F. Acernese *et al.*, Phys. Rev. X **13**, 011048 (2023).
[8] S. E. Woosley, Astrophys. J. **836**, 244 (2017).
[9] S. E. Woosley and A. Heger, Astrophys. J. Lett. **912**, L31 (2021).
[10] R. Farmer, M. Renzo, S. E. de Mink, P. Marchant, and S. Justham, Astrophys. J. **887**, 53 (2019).
[11] R. Farmer, M. Renzo, S. E. de Mink, M. Fishbach, and S. Justham, Astrophys. J. Lett. **902**, L36 (2020).
[12] M. Renzo, R. J. Farmer, S. Justham, S. E. de Mink, Y. Götberg, and P. Marchant, Mon. Not. R. Astron. Soc. **493**, 4333 (2020).
[13] K. Belczynski, R. Hirschi, E. A. Kaiser, J. Liu, J. Casares, Y. Lu, R. O'Shaughnessy, A. Heger, S. Justham, and R. Soria, Astrophys. J. **890**, 113 (2020).

[14] J. S. Vink, E. R. Higgins, A. A. C. Sander, and G. N. Sabhahit, Mon. Not. R. Astron. Soc. **504**, 146 (2021).
[15] G. Costa, A. Bressan, M. Mapelli, P. Marigo, G. Iorio, and M. Spera, Mon. Not. R. Astron. Soc. **501**, 4514 (2021).
[16] D. Gerosa and M. Fishbach, Nat. Astron. **5**, 749 (2021).
[17] Y. Yang, I. Bartos, V. Gayathri, K. E. S. Ford, Z. Haiman, S. Klimenko, B. Kocsis, S. Márka, Z. Márka, B. McKernan, and R. O'Shaughnessy, Phys. Rev. Lett. **123**, 181101 (2019).
[18] U. N. Di Carlo, M. Mapelli, Y. Bouffanais, N. Giacobbo, F. Santoliquido, A. Bressan, M. Spera, and F. Haardt, Mon. Not. R. Astron. Soc. **497**, 1043 (2020).
[19] M. Renzo, M. Cantiello, B. D. Metzger, and Y. F. Jiang, Astrophys. J. Lett. **904**, L13 (2020).
[20] B. J. Carr and S. W. Hawking, Mon. Not. R. Astron. Soc. **168**, 399 (1974).
[21] Y.-F. Cai, X. Tong, D.-G. Wang, and S.-F. Yan, Phys. Rev. Lett. **121**, 081306 (2018).
[22] M. Fishbach, D. E. Holz, and B. Farr, Astrophys. J. Lett. **840**, L24 (2017).
[23] D. Gerosa and E. Berti, Phys. Rev. D **95**, 124046 (2017).
[24] B. P. Abbott, R. Abbott, and T. D. Abbott, Astrophys. J. Lett. **882**, L24 (2019).
[25] R. Abbott, T. D. Abbott, and S. Abraham, Phys. Rev. Lett. **125**, 101102 (2020).
[26] R. Abbott, T. D. Abbott, and S. Abraham, Astrophys. J. Lett. **913**, L7 (2021).
[27] B. Edelman, Z. Doctor, J. Godfrey, and B. Farr, Astrophys. J. **924**, 101 (2022).
[28] Y.-J. Li, Y.-Z. Wang, M.-Z. Han, S.-P. Tang, Q. Yuan, Y.-Z. Fan, and D.-M. Wei, Astrophys. J. **917**, 33 (2021).
[29] A. H. Nitz and C. D. Capano, Astrophys. J. Lett. **907**, L9 (2021).
[30] E. J. Baxter, D. Croon, S. D. McDermott, and J. Sakstein, Astrophys. J. Lett. **916**, L16 (2021).
[31] B. Edelman, Z. Doctor, and B. Farr, Astrophys. J. Lett. **913**, L23 (2021).
[32] M. Fishbach and D. E. Holz, Astrophys. J. Lett. **904**, L26 (2020).
[33] Y.-Z. Wang, S.-P. Tang, Y.-F. Liang, M.-Z. Han, X. Li, Z.-P. Jin, Y.-Z. Fan, and D.-M. Wei, Astrophys. J. **913**, 42 (2021).
[34] C. Kimball, C. Berry, and V. Kalogera, Res. Not. Am. Astron. Soc. **4**, 2 (2020).
[35] C. Kimball, C. Talbot, C. P. L. Berry, M. Zevin, E. Thrane, V. Kalogera, R. Buscicchio, M. Carney, T. Dent, H. Middleton, E. Payne, J. Veitch, and D. Williams, Astrophys. J. Lett. **915**, L35 (2021).
[36] Y.-Z. Wang, Y.-J. Li, and J. S. Vink, Astrophys. J. Lett. **941**, L39 (2022).
[37] J. Golomb and C. Talbot, Phys. Rev. D **108**, 103009 (2023).
[38] V. Tiwari, Astrophys. J. **928**, 155 (2022).
[39] B. Edelman, B. Farr, and Z. Doctor, Astrophys. J. **946**, 16 (2023).
[40] T. A. Callister and W. M. Farr, Phys. Rev. X **14**, 021005 (2024).
[41] M. Zevin, S. S. Bavera, C. P. L. Berry, V. Kalogera, T. Fragos, P. Marchant, C. L. Rodriguez, F. Antonini, D. E. Holz, and C. Pankow, Astrophys. J. **910**, 152 (2021).
[42] V. Tiwari, Classical Quantum Gravity **38**, 155007 (2021).
[43] See Supplemental Material at http://link.aps.org/supplemental/10.1103/PhysRevLett.133.051401 for details, which includes Refs. [44–58].
[44] I. Mandel, W. M. Farr, and J. R. Gair, Mon. Not. R. Astron. Soc. **486**, 1086 (2019).
[45] R. Essick, A. Farah, S. Galaudage, C. Talbot, M. Fishbach, E. Thrane, and D. E. Holz, Astrophys. J. **926**, 34 (2022).
[46] S.-P. Tang, Y.-J. Li, Y.-Z. Wang, Y.-Z. Fan, and D.-M. Wei, Astrophys. J. **922**, 3 (2021).
[47] J. Buchner, PyMultiNest: Python interface for MultiNest, Astrophysics Source Code Library, record ascl:1606.005 (2016), ascl:1606.005.
[48] H. Jeffreys, *Theory of Probability*, 3rd ed (Oxford University Press, New York, 1961).
[49] W. M. Farr, Res. Not. Am. Astron. Soc. **3**, 66 (2019).
[50] C. Talbot and E. Thrane, Astrophys. J. **927**, 76 (2022).
[51] R. Essick and W. Farr, arXiv:2204.00461.
[52] J. Golomb and C. Talbot, arXiv:2210.12287.
[53] J. Golomb and C. Talbot, Astrophys. J. **926**, 79 (2022).
[54] C. Talbot and J. Golomb, Mon. Not. R. Astron. Soc. **526**, 3495 (2023).
[55] S. Galaudage, C. Talbot, T. Nagar, D. Jain, E. Thrane, and I. Mandel, Astrophys. J. Lett. **921**, L15 (2021).
[56] K. K. Y. Ng, S. Vitale, A. Zimmerman, K. Chatziioannou, D. Gerosa, and C.-J. Haster, Phys. Rev. D **98**, 083007 (2018).
[57] S. J. Miller, Z. Ko, T. A. Callister, and K. Chatziioannou, Phys. Rev. D **109**, 104036 (2024).
[58] M. Mould and D. Gerosa, Phys. Rev. D **105**, 024076 (2022).
[59] B. P. Abbott, R. Abbott, and T. D. Abbott, Living Rev. Relativity **23**, 3 (2020).
[60] M. Fishbach and D. E. Holz, Astrophys. J. Lett. **891**, L27 (2020).
[61] Y.-J. Li, Y.-Z. Wang, S.-P. Tang, Q. Yuan, Y.-Z. Fan, and D.-M. Wei, Astrophys. J. Lett. **933**, L14 (2022).
[62] F. Antonini, M. Gieles, F. Dosopoulou, and D. Chattopadhyay, Mon. Not. R. Astron. Soc. **522**, 466 (2023).
[63] F. Antonini and F. A. Rasio, Astrophys. J. **831**, 187 (2016).
[64] H. Tagawa, Z. Haiman, I. Bartos, B. Kocsis, and K. Omukai, Mon. Not. R. Astron. Soc. **507**, 3362 (2021).
[65] V. Gayathri, Y. Yang, H. Tagawa, Z. Haiman, and I. Bartos, Astrophys. J. Lett. **920**, L42 (2021).
[66] M. Mould, D. Gerosa, and S. R. Taylor, Phys. Rev. D **106**, 103013 (2022).
[67] C. L. Rodriguez, M. Zevin, C. Pankow, V. Kalogera, and F. A. Rasio, Astrophys. J. Lett. **832**, L2 (2016).
[68] S. Vitale, S. Biscoveanu, and C. Talbot, Astron. Astrophys. **668**, L2 (2022).
[69] K. Belczynski, A. Heger, W. Gladysz, A. J. Ruiter, S. Woosley, G. Wiktorowicz, H. Y. Chen, T. Bulik, R. O'Shaughnessy, D. E. Holz, C. L. Fryer, and E. Berti, Astron. Astrophys. **594**, A97 (2016).
[70] S. Stevenson, M. Sampson, J. Powell, A. Vigna-Gómez, C. J. Neijssel, D. Szécsi, and I. Mandel, Astrophys. J. **882**, 121 (2019).
[71] T. A. Callister, C.-J. Haster, K. K. Y. Ng, S. Vitale, and W. M. Farr, Astrophys. J. Lett. **922**, L5 (2021).
[72] M. Fishbach and V. Kalogera, Astrophys. J. Lett. **929**, L26 (2022).

[73] R. A. Remillard and J. E. McClintock, Annu. Rev. Astron. Astrophys. **44**, 49 (2006).
[74] M. Gallegos-Garcia, M. Fishbach, V. Kalogera, C. P. L Berry, and Z. Doctor, Astrophys. J. Lett. **938**, L19 (2022).
[75] C. Liotine, M. Zevin, C. P. L. Berry, Z. Doctor, and V. Kalogera, Astrophys. J. **946**, 4 (2023).
[76] A. Ray, I. M. Hernandez, S. Mohite, J. Creighton, and S. Kapadia, Astrophys. J. **957**, 37 (2023).
[77] J. Godfrey, B. Edelman, and B. Farr, arXiv:2304.01288.
[78] A. Ray, I. Magaña Hernandez, K. Breivik, and J. Creighton, arXiv:2404.03166.
[79] D. Gerosa, E. Berti, R. O'Shaughnessy, K. Belczynski, M. Kesden, D. Wysocki, and W. Gladysz, Phys. Rev. D **98**, 084036 (2018).
[80] Y.-J. Li, S.-P. Tang, S.-J. Gao, D.-C. Wu, and Y.-Z. Wang, arXiv:2404.09668.
[81] W. M. Farr, M. Fishbach, J. Ye, and D. E. Holz, Astrophys. J. Lett. **883**, L42 (2019).
[82] J. M. Ezquiaga and D. E. Holz, Phys. Rev. Lett. **129**, 061102 (2022).
[83] R. Abbott, H. Abe, F. Acernese, K. Ackley, N. Adhikari, and Adhikari, Astrophys. J. **949**, 76 (2023).
[84] Y.-J. Li, S.-P. Tang, Y.-Z. Wang, and Y.-Z. Fan, arXiv:2406.11607.
[85] https://github.com/JackLee0214/Resolving-the-stellar-collapse-and-hierarchical-merger-origins-of-the-coalescing-black-holes
[86] https://www.gw-openscience.org
[87] https://github.com/ColmTalbot/gwpopulation